Biomaterials Science

ROYAL SOCIETY OF CHEMISTRY

PAPER

View Article Online
View Journal | View Issue

Cite this: *Biomater. Sci.*, 2025, **13**, 5813

Harnessing the synergy of copper nanoparticles and vitamin C towards the resolution of wound infection

Alhussain Ojaym,[a,b] Trae Hillyer,[c] Guanyu Chen,[d] Songping D. Huang,[d] Woo Shik Shin†[c] and Min-Ho Kim *†[a,e]

Copper ions have been considered to hold promise for the treatment of wound infections due to their unique characteristics that exhibit not only antibacterial activities through multiple bactericidal mechanisms but also tissue reparative activities by acting as a co-factor for many angiogenic promoters and enzymes. However, higher doses are necessary to achieve sufficient bactericidal and antibiofilm effects. The objective of this study is to develop copper nanoparticles (CuNPs) as an antimicrobial agent by harnessing the characteristics of copper and vitamin C (VC) to form a sustained catalytic cycle, leading to a significant enhancement of bactericidal and antibiofilm effects when compared with the use of CuNPs alone. Specifically, our results demonstrate that CuNPs, when properly combined with a high dose of VC (>1 mM), can synergistically enhance antibacterial activity by increasing the generation of intracellular reactive oxygen species (ROS) in bacterial cells, effectively targeting a broad spectrum of bacteria. Additionally, the use of Pluronic F-127 gel has made it facile for encapsulating a defined amount of CuNP and VC to the hydrogel for topical application, which exhibits potent antibacterial and antibiofilm effects assessed by well diffusion assay and colony biofilm assay, respectively. Finally, the *in vivo* evaluation of antimicrobial efficacy in the murine model of skin wound infection by *S. aureus* and *P. aeruginosa* confirms that the topical application of F-127/CuNPs/VC hydrogel can significantly reduce the bacterial burden, demonstrating the therapeutic potential of F-127/CuNPs/VC hydrogel in treating wound infections.

Received 19th June 2025,
Accepted 26th August 2025

DOI: 10.1039/d5bm00933b

rsc.li/biomaterials-science

1. Introduction

Wound healing is a complex and dynamic process involving a spatiotemporally orchestrated integration of multiple cellular and molecular events.[1,2] Acute wounds are healed by following the normal process of repair including inflammation, proliferation, and remodeling phases. However, unresolved bacterial infection can impede the normal process of wound healing and lead to wound chronicity.[3] In particular, the formation of bacterial biofilm plays a significant role in the pathogenesis of wound chronicity associated with the capacity of biofilm bacteria to evade the attack by innate immune system and develop resistance to traditional antibiotics therapies.[4–6] Importantly, biofilm infections in chronic wounds are frequently associated with colonization by multispecies bacteria including both Gram-positive and Gram-negative bacteria. The common bacteria involved in chronic skin wounds include *Staphylococcus aureus* (*S. aureus*), *Pseudomonas aeruginosa* (*P. aeruginosa*), and *Acinetobacter baumanii* (*A. baumanii*).[7–9] Despite the development of novel antimicrobial agents, the cost and complexity of treating chronic wounds associated with biofilm infections remain a serious challenge.

To address this, metal ions, including zinc, iron, silver and copper, have been exploited as alternative antimicrobial agents due to their potent antibacterial properties that trigger the generation of reactive oxygen species (ROS).[10–12] Among them, copper ions have been considered to hold promise for the treatment of wound infections. This has been associated with their unique characteristics that exhibit not only antibacterial activities through multiple bactericidal mechanisms[13,14] but also tissue reparative activities by acting as a co-factor for many angiogenic promoters and mediators.[15,16] These multifaceted effects of copper ions render them to be a potent agent for the healing of an infected chronic wound. However, up to

[a]*School of Biomedical Sciences, Kent State University, Kent, OH 44242, USA*
[b]*Department of Medical Laboratory Technology, Faculty of Applied Medical Science, University of Tabuk, Tabuk, Saudi Arabia*
[c]*Department of Pharmaceutical Sciences, College of Pharmacy, Northeast Ohio Medical University, Rootstown, OH 44272, USA*
[d]*Department of Chemistry and Biochemistry, Kent State University, Kent, OH 44242, USA*
[e]*Department of Biological Sciences, Kent State University, Kent, OH 44242, USA. E-mail: mkim15@kent.edu; Fax: +1 330-672-3713; Tel: +1 330-672-1445*
† Equally contributed to this work.

now, there has been no copper-based drug as an antibacterial, antifungal or antiviral agent used in the clinic. The main reason stems from the fact that copper is an essential metal for all forms of organisms due to its role as a catalytic and structural cofactor for many proteins and enzymes. However, when it is unbound to proteins or enzymes, the free copper ion can exhibit deleterious effects due to its ability to trigger Fenton-like reactions that produce hydroxyl radicals to cause oxidative damage to proteins, lipids, and nucleic acids.[17] Under normal conditions, copper is sequestered and tightly regulated at every stage of its uptake, transport, delivery and excretion in cells to achieve copper homeostasis in order to prevent oxidative stress.[18] To circumvent the cellular homeostatic regulation of copper in bacteria, the development of copper nanoparticles (CuNPs) has been widely investigated for the purpose of achieving sustained and slow release of copper ions to wound sites. However, the use of copper-based nanoparticles requires higher doses, *i.e.*, in the millimolar range to ensure sufficient bactericidal effects,[19–21] which can cause cytotoxicity to host tissue. Thus, there is still a scientific gap to overcome the limitations of copper-based nanoparticles for wound infection application.

In this study, we have developed a new strategy to harness the synergy of CuNPs and vitamin C (VC) towards the enhanced antibacterial and antibiofilm effects against broad-spectrum bacteria. Our strategy is to use VC as a co-drug (*i.e.*, a reducing agent) to form a sustained Cu(0)/Cu(I)/Cu(II) redox cycle that boosts the production of ROS.[22] The use of VC as a sacrificial reducing agent allows CuNPs to be continually recycled as a catalyst rather than to be consumed in the Fenton-like catalytic reaction. VC not only enhances the antibacterial activity of CuNPs by regenerating Cu(I) and Cu(0) and maintaining the redox cycle, but also protects mammalian cells from oxidative damage due to its potent antioxidant properties.[23] The anti-infective efficacy of CuNPs in combination with VC have been assessed using a series of *in vitro* studies as well as *in vivo* study involving a murine model of skin wound infection. Our results demonstrate a synergistic effect of CuNPs and VC in conferring antibacterial and antibiofilm activity against broad-spectrum of infections induced by Gram-positive and Gram-negative bacteria.

2. Materials and methods

2.1. Synthesis of CuNPs

CuNPs were synthesized using a green hydrothermal synthesis method using copper(II) chloride ($CuCl_2{\cdot}2H_2O$) as a starting material. L-Ascorbic acid (VC) was used as a reducing as well as capping agent. Briefly, a 4 mM of $CuCl_2{\cdot}2H_2O$ (Sigma-Aldrich) solution was prepared by dissolving the copper salt in 18 mL of N_2 purged deionized water containing 360 mg of polyvinylpyrrolidone (PVP, MW = 8000). Varying amounts of L-ascorbic acid (VC) were added to the solution and the mixture was thoroughly stirred until the VC was completely dissolved. The concentrations of VC in the mixture were adjusted to 0.4 M, 1.2 M, 2.0 M, and 4 M. These mixtures were then transferred to autoclave and heated in an oven at 120 °C for four hours. The resulting suspensions were cooled to room temperature over 24 hours to afford CuNPs with different sizes. The synthesized CuNPs were then transferred to glass tubes and filtered using a 0.2 μm membrane filter to remove impurities. The solution was added with acetone to purify CuNPs by centrifuging at 4500 rpm for 25 minutes. The purified CuNPs were suspended in deionized water and stored in a refrigerator (4 °C). Such CuNPs were found to be stable and active for up to two weeks under these conditions.

2.2. DLS characterization of CuNPs

The hydrodynamic sizes of CuNPs were determined by Dynamic Light Scattering (DLS). The CuNPs were dispersed in deionized water, and the suspension was sonicated for 10 minutes to provide uniform dispersion. Measurements were performed on a Malvern Zetasizer Nano at 25 °C, with the detector positioned at an angle of 90° (Backscatter). Each sample was analyzed in triplicate to increase accuracy, and measurements of hydrodynamic diameter and polydispersity index (PDI) were obtained from the DLS software.

2.3. TEM characterizations of CuNPs

The morphology of CuNPs was imaged by Transmission Electron Microscopy (TEM) using a FEI Tecnai G2 F20 microscope. The samples were dispersed in ethanol by mild ultra-sonication for ~5–10 wt% prior to TEM analysis and then the samples were deposited on a 200-mesh copper grid coated with Lacey carbon (Ted Pella) by dipping the sample into suspension, followed by drying under vacuum at 100 °C for one hour.

2.4. Determination of minimum inhibitory concentration (MIC)

The antibacterial activity of CuNPs was assessed for various bacterial strains including both laboratory and clinical isolates. The laboratory bacterial strains used include methicillin-sensitive *S. aureus* (MSSA, ATCC 6538), methicillin-resistant *S. aureus* (MRSA, ATCC BAA-44), drug-sensitive *P. aeruginosa* (DSPA, ATCC 15692) and drug-resistant *P. aeruginosa* (DRPA, ATCC BAA-2108). The clinical isolates (obtained from Dr Robert Bonomo at Case Western Reserve University) include *S. aureus* (SA-1622 and SA-1624 strains), *P. aeruginosa* (PA-VA 12 and PA-VA 50 strains), *Acinetobacter baumannii* (AB1-PR328 strain). The minimum inhibitory concentration (MIC) of CuNPs was determined using the broth microdilution method, following the guidelines by the Clinical and Laboratory Standards Institute (CLSI). For this, a chosen bacterial strain was prepared at a concentration of 10^6 CFU mL^{-1} in a 96 well-plate and varying concentrations of CuNPs alone or in combination with VC were added to the wells with bacteria. The bacteria were incubated at 37 °C for 24 hours and the lowest concentration of CuNPs at which no visible growth of bacteria was observed was considered as the MIC.

2.5. Measurement of intracellular ROS

The level of intracellular ROS was quantified using the dichloro-dihydro-fluorescein diacetate (DCFH-DA, Sigma-Aldrich) assay in *S. aureus*, *P. aeruginosa*, and human dermal fibroblasts (HDFs). Bacteria (1×10^6 CFU mL^{-1}) and HDFs (at a density of 40 000 cells per well) were seeded in 96-well plate and incubated with varying concentrations of VC (0–4 mM) at 40 μM CuNPs for 3 hours. The cells were then incubated with PBS containing 20 μM DCFH-DA for 30 min at 37 °C. After the incubation, cells were washed twice to remove excessive fluorescent dye, and the fluorescence intensity was quantified using a spectrophotometer at the excitation and emission wavelengths of 497 nm and 529 nm, respectively.

2.6. Dose-dependent antibacterial activity of CuNPs

The dose-dependent antibacterial activity of CuNPs was determined against *S. aureus* and *P. aeruginosa* using a colony-forming unit (CFU) assay. Varying concentrations of CuNPs (0, 20, 40, and 80 μM) mixed with VC at 10 mM concentration were transferred to the solution of bacteria (1×10^6 CFU mL^{-1}) prepared in 96-well plate and the bacterial cells were incubated at 37 °C for 24 hours. After the incubation, bacterial cells were serially diluted with sterile PBS and 50 μL of each dilution was plated on tryptic soy agar plates. The number of bacteria was determined by CFU counting.

2.7. Preparation of Pluronic F-127 hydrogel loaded with CuNPs and VC

The Pluronic F-127 hydrogel loaded with CuNPs and VC (F-127/CuNPs/VC) was prepared by the cold method, in which separately prepared quantity of CuNPs and VC were mixed with F-127 solution by gently stirring them at 4 °C. The F-127 solution was prepared by gradually dissolving a defined amount of Pluronic F-127 (molecular weight of 12 600 g mol^{-1}, Sigma-Aldrich) and propylene glycol in distilled water at 4 °C. The concentration of Pluronic F-127 in hydrogel was maintained at 25% (w/v) since this concentration was shown to exhibit fast gelation at 37 °C and suitable viscoelastic properties.[24] The concentration of CuNPs and VC was maintained at 100 μg g^{-1} and 10%, respectively.

2.8. Cytotoxicity of F-127/CuNPs/VC hydrogel

The cytotoxicity of F-127/CuNPs/VC hydrogel was assessed using the medium extraction method described previously.[25] The medium extracts were obtained by incubating various formulation of hydrogels (F-127, F-127 with CuNPs, F-127 with VC, or F-127 with CuNPs and VC) in DMEM for 24 hours at 37 °C and the extracts were filtered through a 0.45 μm pore size filter (Millipore membrane filter, Sigma-Aldrich). Then, the extracted medium was treated to HDFs prepared in 96-well plate at a density of 4×10^5 cells per well and the cells were incubated for 24 hours. The cytotoxicity of each hydrogel formulation was examined by MTT assay by following the manufacture protocol (Trevigen, Gaithersburg, MD).

2.9. Release of VC from F-127 hydrogel

The *in vitro* release of VC from the prepared hydrogel formulations was examined using a dialysis membrane approach with some modifications.[26] The dialysis membranes (12 kDa CelluSep, Sigma-Aldrich) were preconditioned in Milli-Q water for 1 hour, followed by thorough rinsing to empty residual preservatives. Subsequently, 2 mL of hydrogel solution, pre-mixed with VC, was loaded into the dialysis membrane at 4 °C, which served as the donor compartment. The dialysis membrane was securely sealed to prevent leakage and immersed in a 50 mL receptor compartment containing 15 mL of phosphate-buffered saline (PBS; pH 7.4, Gibco-tm) as the release medium. The receptor compartment was maintained at 37 ± 0.5 °C in a thermostatically controlled shaking incubator set to 70 rpm to simulate physiological conditions. At selected time points (1, 2, 3, 4, 6, 8, 10, and 24 hours), 2 mL aliquots were withdrawn from the receptor compartment and immediately replaced with an equal volume of fresh PBS pre-equilibrated to 37 °C to maintain consistent experimental conditions. The concentration of VC in the collected samples was quantified using an Ascorbic Acid Assay Kit (Abcam, cat no.: ab65346). The release data were normalized to the initial VC content and expressed as the cumulative percentage of VC released over time.

2.10. Well diffusion assay

Bacterial strains including *S. aureus* and *P. aeruginosa* were cultured overnight at 37 °C, and the suspensions were diluted to obtain a final concentration of 1×10^6 CFU mL^{-1}. Wells with a diameter of 6 mm were aseptically punched into the agar using a sterile biopsy punch. A volume of 100 μL of different F-127 hydrogel formulation was placed to a well. The hydrogel formulation includes negative control (F-127 hydrogel only), positive control (F-127 Hydrogel with 1% ciprofloxacin, F-127/CIP), F-127 hydrogel with CuNP (F-127/CuNPs), F-127 hydrogel with VC (F-127/VC), and F-127 hydrogel with CuNP and VC (F-127/CuNPs/VC). The agar plate was incubated for 24 hours at 37 °C and the zones of inhibition formed around the well was measured.

2.11. The antibiofilm effect of F-127/CuNPs/VC hydrogel *in vitro*

Biofilms of *S. aureus* and *P. aeruginosa* were formed by following the colony biofilm model as previously described.[27] In brief, bacterial suspension was prepared in fresh nutrient broth at a concentration of 1.5×10^5 CFU mL^{-1}. A 50 μL of the bacterial suspension was inoculated to a sterilized membrane filter with 25 mm in diameter and 0.2 μm in pore size (Whatman cellulose nitrate membrane, Tisch Scientific). Then, the membrane filter was placed onto nutrient agar plate and incubated for 24 hours at 37 °C to allow the formation of biofilm. To evaluate the antibiofilm effects of various hydrogel formulation, a 100 μL volume of varying F-127 hydrogel formulation was gently applied on top of the established biofilm and incubated for 24 hours at 37 °C. The hydrogel formulation

treated to the biofilm includes negative control (F-127 hydrogel only), positive control (F-127 Hydrogel with 1% ciprofloxacin, F-127/CIP), F-127 hydrogel with CuNP (F-127/CuNPs), F-127 hydrogel with VC (F-127/VC), and F-127 hydrogel with CuNPs and VC (F-127/CuNPs/VC). After a further 24 h incubation, the biofilm was stripped off from the membrane in 15 mL PBS supplemented with Tween 80 (0.5% w/v) by a series of vertexing (1 min) and sonication (15 min). Then, the bacterial suspension was serially diluted and plated on fresh nutrient agar for standard CFU counting.

2.12. Antibacterial efficacy of F-127/CuNPs/VC hydrogel *in vivo*

In this study, Jax Swiss outbred mice (male and female mice, 4–5 months old, Jackson Laboratory) were used to assess the antibacterial efficacy of F-127/CuNPs/VC hydrogel in a wound infection model. A full-thickness circular wound was created on the dorsal surface of mouse using a sterile biopsy punch (5 mm). The wound was coated with a Tegaderm® dressing to form a transparent and semipermeable layer and subsequently 40 μL of bioluminescent *S. aureus* (Xen 36, 5×10^6 CFU mL^{-1}) or *P. aeruginosa* (Xen 41, 5×10^6 CFU mL^{-1}) suspended in PBS was introduced into the wound site under the dressing as described in our recent study.[28] On day 1 and day 2 post-infection, a defined dose of F-127/CuNPs/VC hydrogel or vehicle control (F-127 hydrogel) was topically applied to the wounds of either the treatment group or the vehicle control group. Wound bacterial burden was imaged using the IVIS system. The experimental groups used in this study include, (1) *S. aureus* + vehicle (F-127), (2) *S. aureus* + F-127/CuNPs/VC hydrogel, (3) *P. aeruginosa* + vehicle (F-127), and (4) *P. aeruginosa* + CuNPs/VC/F-127 hydrogel. All animal procedures were performed in accordance with the Guide for Care and Use of Laboratory Animals and approved by the Institutional Animal Care & Use Committee (IACUC) of the Northeast Ohio Medical University.

2.13. Statistical analysis

Statistical analysis was performed by using GraphPad Prism 10. Data were presented as means ± standard deviation (SD). Statistical analysis was performed by using two-tailed Students *T*-test (for two groups) or ANOVA (for more than two groups). For all the analysis, *p*-value of less than 0.05 was considered to be statistically significant.

3. Results and discussion

3.1. Synthesis and characterization of CuNPs

CuNPs were synthesized by a green hydrothermal synthesis method using VC as a reducing as well as capping agent[29] (Fig. 1a). Adjusting the molar ratio between $CuCl_2$ and VC resulted in the synthesis of CuNPs with different sizes. When the amounts of VC added to the given $CuCl_2$ solution

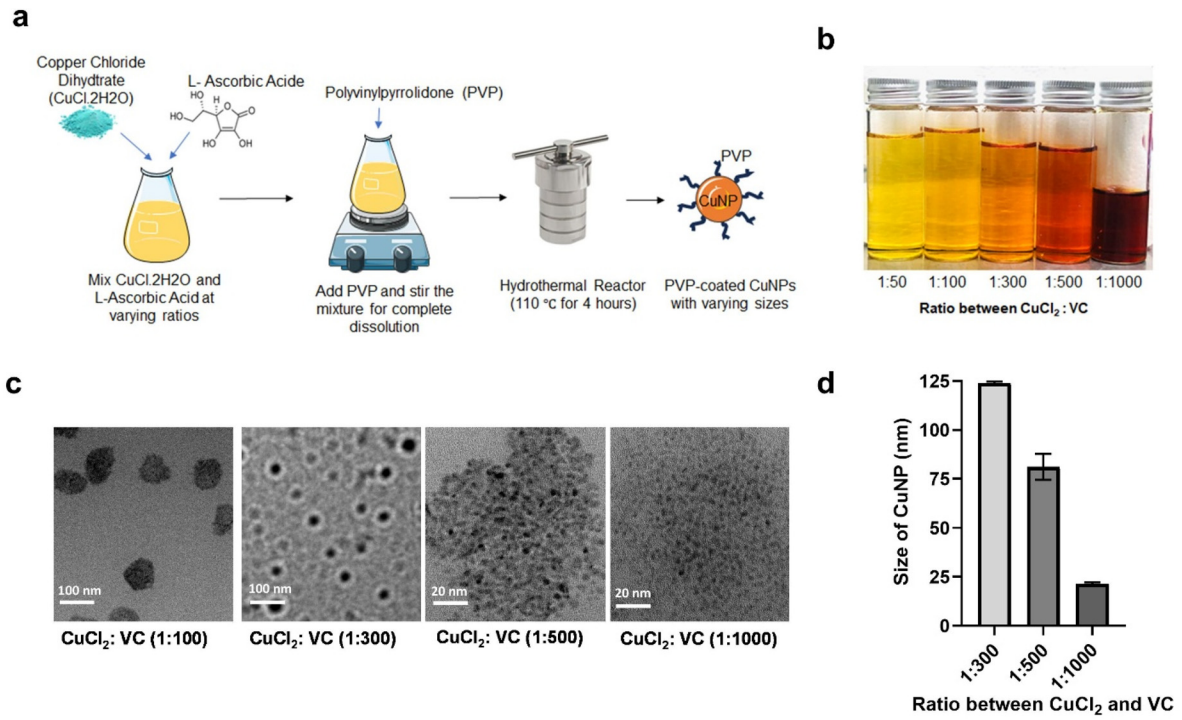

Fig. 1 Synthesis and characterization of CuNPs. (a) Schematic illustration of the synthesis of CuNPs. (b) Changes in color of CuNPs synthesized with varying ratios of $CuCl_2$to VC. (c) TEM images of CuNPs with different sizes obtained by changing the ratio of $CuCl_2$ to VC. The TEM images were cropped from the original images. See Fig. S1 for the original uncropped images of CuNPs. (d) Determination of the size of different CuNPs obtained by changing the ratio of $CuCl_2$ to VC by DLS measurements.

increased (ratio of 1 : 100, 1 : 300, 1 : 500, and 1 : 1000 between $CuCl_2$ and VC), the solution gradually darkened from yellow to dark brown, suggesting the increased accumulation of Cu(0) in the catalytic cycle (Fig. 1b). This change in color is indicative of the reduction process of Cu(II) ions to Cu(0) nanoparticles. The synthesized CuNPs were characterized by transmission electron microscopy (TEM) and dynamic light scattering (DLS) methods. TEM images revealed a spheroidal morphology of synthesized CuNPs in which the sizes of particles were decreased with increasing the molar ratio between $CuCl_2$ and VC (Fig. 1c and Fig. S1). Further characterization by DLS measurements revealed that a ratio of 1 : 300 yielded CuNPs with a mean hydrodynamic diameter of 120 nm. Further increasing the amount of VC with ratios of 1 : 500 and 1 : 1000 yielded particles with mean hydrodynamic diameters of 80 nm and 20 nm, respectively (Fig. 1d). This size reduction with increasing VC concentration suggests that VC played an important role in the nucleation and growth phases of the particles as a reducing and capping agent. For example, VC reduces Cu(II) to Cu(I) and Cu(0), creating high nucleation rate, which generates many small copper nuclei. As the copper atoms are distributed across many nuclei, particle growth is limited, resulting in smaller nanoparticles. Additionally, VC acts as a capping agent, stabilizing the nanoparticles and preventing further aggregation by the Ostwald ripening, thereby stabilizing smaller nanoparticles.

3.2. Effect of VC on CuNPs-mediated Fenton-like catalytic reactions for ROS generation

Both Cu(I) and Cu(0) ion can generate ROS in cells by triggering the Fenton-like catalytic reactions involving the Cu(0)/Cu(I)/Cu(II) redox cycle.[17,30] The well-known Fenton-like catalytic reactions of copper consist of three steps, where steps [1] and [2] produce free radicals, while step [3] consumes them[22,31,32] (Fig. 2a). We hypothesized that if an external sacrificial reducing agent such as VC is added to this catalytic cycle, Cu(I) can be readily recycled back to Cu(0) by the reducing agent. Likewise, Cu(II) can also be turned back to Cu(I) and/or Cu(0) by the same reducing agent without consuming free radicals and thus form a sustaining Cu(0)/Cu(I)/Cu(II) redox cycle that boosts the production of cellular ROS. To test this, we examined whether a combined treatment of VC could

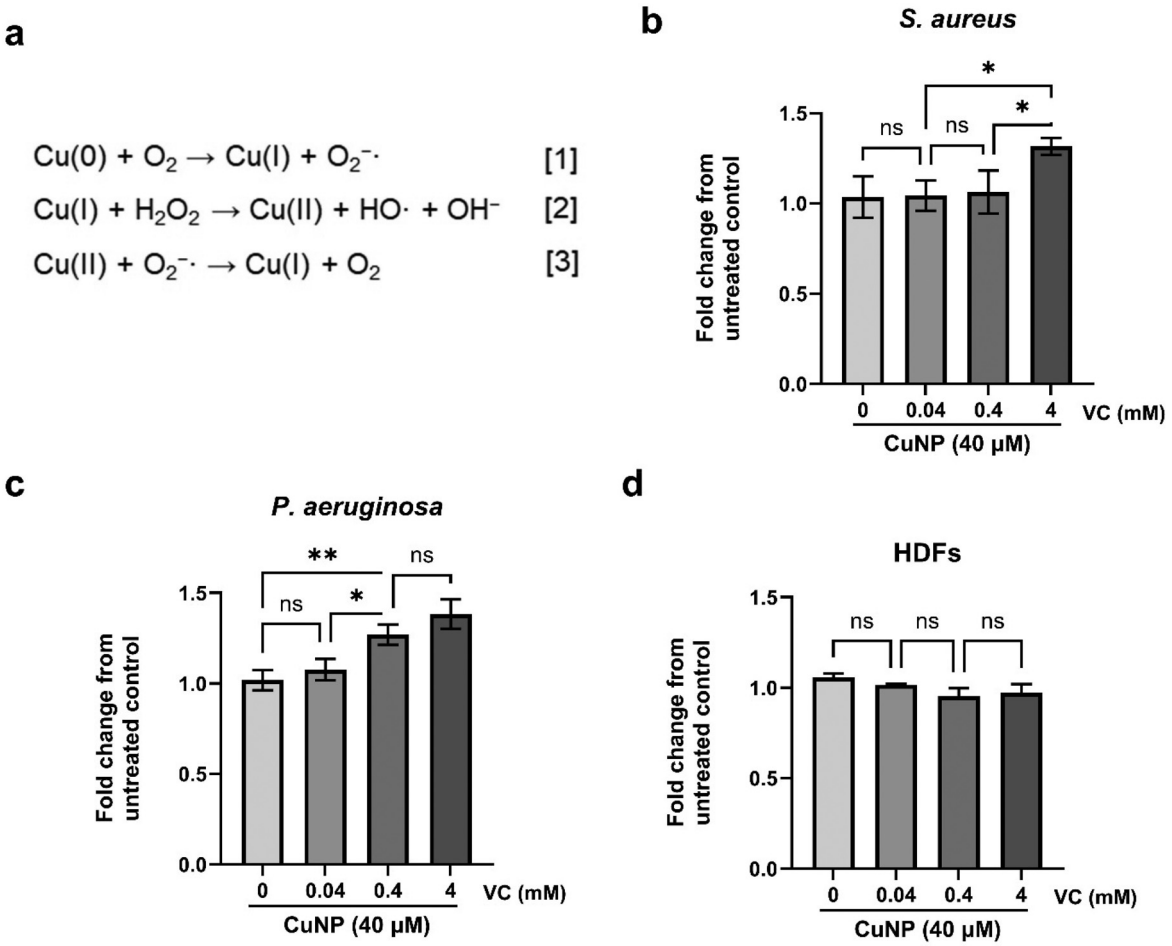

Fig. 2 The Effect of VC on CuNPs-dependent Fenton-like reactions for intracellular ROS generation. (a) A diagram showing copper-driven Fenton-like reactions that lead to the ROS generation. (b–d) The ROS levels in (b) *S. aureus*, (c) *P. aeruginosa*, and (d) HDFs treated with CuNPs (40 μM, 80 nm in size) with varying concentrations of VC (0–4 mM).

enhance CuNPs-induced production of intracellular ROS in bacterial cells. The extent of ROS generation in bacterial cells was compared with that in mammalian cells using human dermal fibroblast cells (HDFs). For this, intracellular ROS levels were measured with increasing concentrations of VC in *S. aureus* and *P. aeruginosa* at the fixed concentration of CuNPs at 40 μM. Either CuNPs or VC alone did not alter ROS levels in *S. aureus* and *P. aeruginosa*, compared to an untreated control group (Fig. S2). The treatment of CuNPs in combination of VC up to 0.4 mM did not increase ROS levels in *S. aureus* compared to an untreated control group. However, further increasing the concentration of VC to 4 mM significantly increased intracellular ROS generation in *S. aureus* (Fig. 2b). Interestingly, ROS generation in *P. aeruginosa* occurred at the 10-fold lower concentration of VC at 0.4 mM (Fig. 2c), suggesting that Gram-negative *P. aeruginosa* bacteria are more susceptible to CuNPs and VC-mediated ROS generation than Gram-positive *S. aureus* bacteria.

By observing the capability of VC in boosting CuNPs-mediated ROS generation in bacteria, we subsequently examined whether CuNPs and VC could also generate ROS in mammalian cells using HDFs. There was no significant increase in ROS levels in HDFs for all the VC concentration used in *S. aureus* and *P. aeruginosa* (Fig. 2d), suggesting that mammalian cells are less susceptible to CuNPs/VC-induced reaction. Although the detailed mechanism remains to be further elucidated, it is likely that bacterial cells might possess fewer antioxidant mechanisms than mammalian cells, suggesting that bacterial cells are likely to be more susceptible to ROS damage than mammalian cells. For example, bacteria have a simpler cell structure, making them more vulnerable to damage from ROS. Compared to mammalian cells, bacteria typically have less repertoire of antioxidant enzymes including superoxide dismutase (SOD) and catalase (CAT)[33,34] than mammalian cells, which utilize multiple antioxidant enzymes including glutathione peroxidase (GPx), thioredoxin peroxidase (TPx), and peroxiredoxins (Prx), in addition to SOD and CAT.[35,36] It is also possible that mammalian cells readily utilize VC as an antioxidant and thereby neutralize ROS.[37]

3.3. Antibacterial efficacy of CuNPs/VC cocktail against broad-spectrum bacteria

By observing the capability of CuNPs to elicit the Fenton-like reaction to generate ROS when combined with higher dose of VC, we next sought to determine the range of the concentrations of CuNPs and VC that can be applied to mammalian cells without eliciting an overt toxicity. This was conducted using a live/dead viability assay in HDFs. The viability assay revealed that VC at concentrations up to 25 mM could be used without eliciting a toxicity (Fig. S3a). CuNPs did not elicit a significant toxicity at concentrations up to 200 μM in HDFs (Fig. S3b). By determining the threshold of CuNPs and VC doses that do not elicit a toxicity on mammalian cells, we next examined whether CuNPs and VC used within the threshold doses would exhibit synergistic antibacterial effects by determining their MIC values against varying bacterial strains.

Table 1 MIC values of CuNPs for against several different bacterial strains (the MICs were obtained in the presence of VC at 10 mM)

	Bacterial strains	MIC (μM)
Laboratory strains	Methicillin-sensitive *S. aureus* (ATCC 6538)	20
	Methicillin-resistant *S. aureus* (ATCC BAA-44)	10
	Drug-sensitive *P. aeruginosa* (ATCC 15692)	1.25–2.5
	Drug-resistant *P. aeruginosa* (ATCC BAA-2108)	1.25–2.5
Clinical isolates	*S. aureus* (SA-1622)	20
	S. aureus (SA-1624)	20
	P. aeruginosa (PA-VA12)	80
	P. aeruginosa (PA-VA50)	40
	Acinetobacter baumannii (AB1-PR309)	80
	Acinetobacter baumannii (AB1-PR328)	40

Either CuNPs alone up to 160 μM or VC alone up to 25 mM did not exhibit any discernable antibacterial activity (data not shown). On the other hand, CuNPs exhibited antibacterial effects when combined with 10 mM VC against various bacterial strains including laboratory strains as well as clinical isolates of bacteria (Table 1 and Fig. S4). The MIC values of CuNPs for Gram-positive bacteria including methicillin-sensitive *S. aureus* (MSSA) and methicillin-resistant *S. aureus* (MRSA) were measured to be 20 μM in the presence of 10 mM VC. The antibacterial effect of CuNPs was more effective against Gram-negative *P. aeruginosa*, in which MICs of CuNPs were determined to be 1.25–2.5 μM for drug-susceptible *P. aeruginosa* (DSPA) and drug-resistant *P. aeruginosa* (DRPA). To evaluate the broad-spectrum antibacterial efficacy of CuNPs/VC cocktail, MIC values were also determined against several clinical isolates of bacteria, which include *S. aureus* (SA-1622 and SA-1624), *P. aeruginosa* (PA-VA 12 and PA-VA 50), and *Acinetobacter baumannii* (AB1-PR328). The results showed that the CuNPs/VC cocktail was also effective against such clinical isolates with the measured MIC values ranging from 40 to 80 μM, albeit these MIC values were found to be somewhat higher than those overserved for the laboratory strains of bacteria.

By determining the MIC values of CuNPs for varying bacterial strains, we next examined whether CuNPs could exhibit dose-dependent antibacterial effects. This was assessed by counting colony forming units (CFUs) from both *S. aureus* and *P. aeruginosa* treated with increasing doses of CuNPs in the presence of VC at 10 mM. The numbers of CFU for both bacteria concomitantly decreased with increasing concentration of CuNPs, by reaching about 5-log reduction of CFU at the four times their MIC doses (80 μM for *S. aureus* and 5 μM for *P. aeruginosa*) (Fig. 3). These findings confirm that CuNPs when combined with VC can exert bactericidal effects *via* a dose-dependent manner.

Collectively, our findings support that CuNPs combined with a high concentration of VC (>10 mM) could be highly effective against a broad spectrum of bacterial pathogens. The synergy of CuNPs and VC was confirmed by checkerboard assay, in which fractional inhibitory concentration (FIC) index values were calculated to be 0.33 for *S. aureus* and 0.4 for *P. aeruginosa*, suggesting the synergism between CuNPs and

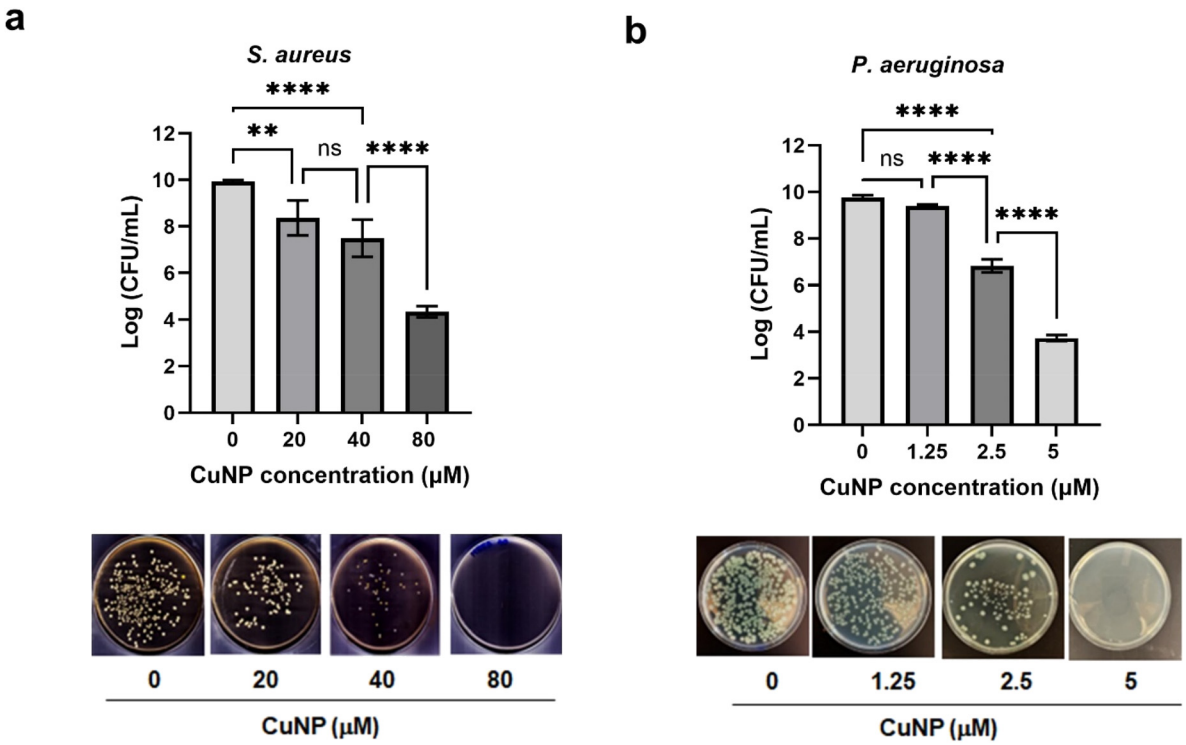

Fig. 3 Dose-dependent antibacterial activity of CuNPs combined with VC against *S. aureus* and *P. aeruginosa*. (a) The antibacterial activity of CuNPs (80 nm in size) against *S. aureus* (ATCC 6538) with varying concentrations (0–80 μM) in the presence of 10 mM VC. (b) The antibacterial activity of CuNPs (80 nm in size) against *P. aeruginosa* (ATCC 15692) with varying concentrations (0–5 μM) in the presence of 10 mM VC. The antibacterial activity was quantified by log colony forming units (log CFU). $^{**}p < 0.01$, $^{****}p < 0.0001$. n.s: not significant.

VC in conferring antibacterial effects (Table S1). The MIC values of CuNPs have been reported to be at millimolar ranges to ensure sufficient antibacterial effects.[19–21] Our results demonstrate that the use of VC as a sacrificial reducing agent allowed CuNPs to be continually recycled as a catalyst rather than to be consumed in the Fenton-like catalytic reaction. This resulted in a dramatic decrease in the concentration of copper required for achieving antibacterial effects to micromolar ranges.

3.4. A facile preparation of injectable hydrogel scaffold for encapsulating CuNPs and VC

After observing the potent antibacterial effects of CuNPs/VC, we next engaged in a study to develop a strategy for controlled delivery of CuNPs and VC under *in vivo* conditions. For this, we employed a Pluronic F-127 thermo-reversible hydrogel as a vehicle for the delivery of CuNPs and VC. Pluronic F-127 hydrogel is attractive as an injectable hydrogel due to their biocompatibility and temperature-sensitive sol–gel properties that hold promise.[38,39] At temperature below the lower critical solution temperature (LCST), F-127 is in a solution state and the solution becomes hydrogel at temperature above the LCST.[38] This thermos-reversible property of F-127 gel makes it facile for encapsulating a defined amount of CuNPs and VC within the gel (Fig. 4a). In this study, 25% concentration of Pluronic F-127 was selected to ensure the gradual and sustained release profile of CuNPs and VC as well as hydrogel stability.[24] The formulation of VC in this hydrogel was maintained at 10% since up to 20% concentrations of VC have been shown to be non-toxic for topical applications.[40] Although the VC encapsulated in the hydrogel was released rapidly to as much as 70% during the initial one hour, this was followed by gradual release over the course of 24 hours (Fig. 4b). We next assessed the cytotoxicity of Pluronic F-127 gel with CuNPs and VC (F-127/CuNPs/VC) on HDFs using an MTT assay, in which the extracts of the hydrogel were treated to HDFs, and the cell viability was determined after 24 hours. The F-127/CuNP/VC hydrogel exhibited a low toxicity on HDFs as quantified by percentage cell viability (Fig. 4c), suggesting a suitable biocompatibility of F-127/CuNP/VC hydrogel.

3.5. Antibacterial efficacy of the F-127/CuNPs/VC hydrogel

After formulating F-127/CuNP/VC hydrogel for topical application, we next assessed its antibacterial efficacy against two common bacterial pathogens found in chronic skin wounds, *S. aureus and P. aeruginosa*. This was tested using a standard well disc diffusion assay for three different formulations of hydrogel, which include F-127 hydrogel with CuNPs (F-127/CuNP), F-127 hydrogel with VC (F-127/VC), and F-127 hydrogel with both CuNPs and VC (F-127/CuNP/VC). The F-127 hydrogel without CuNPs and VC was used as a vehicle control. The

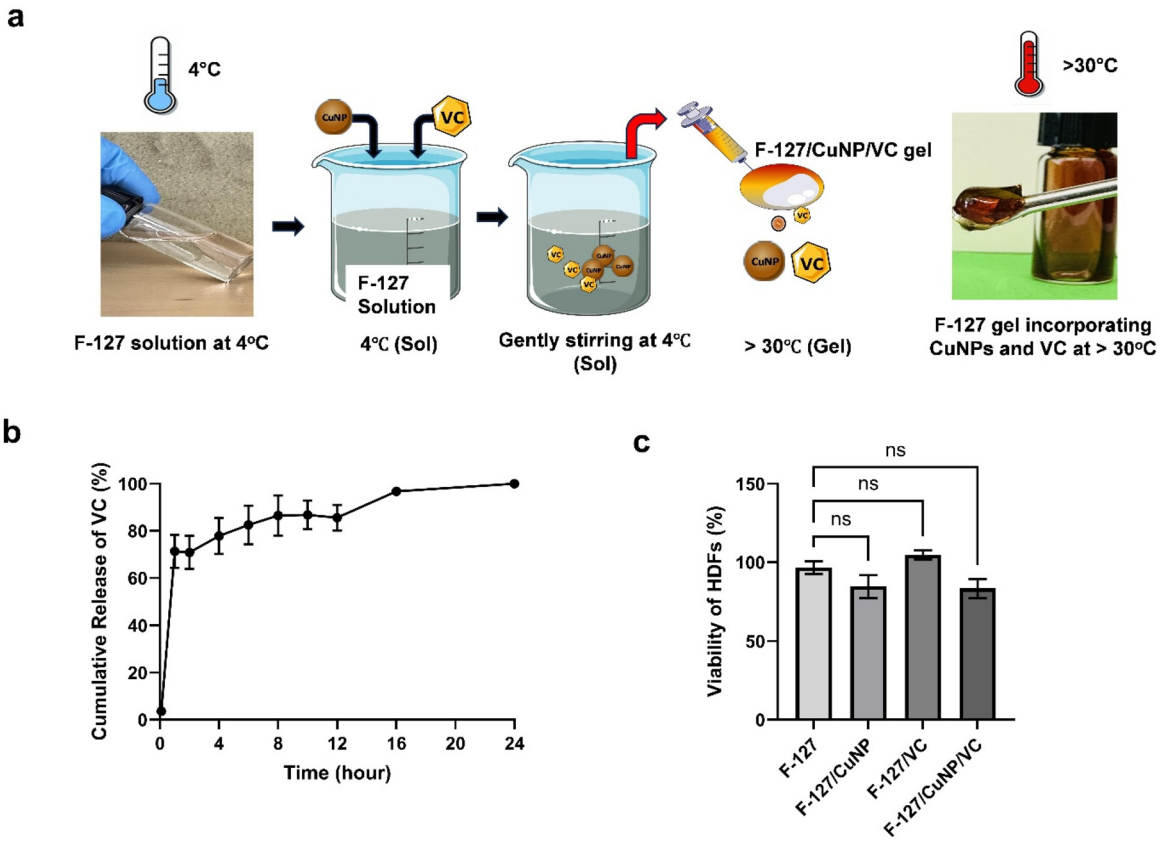

Fig. 4 Preparation of injectable hydrogel for encapsulating CuNPs and VC. (a) A schematic illustration of the preparation of injectable hydrogel based on Pluronic F-127 (25% w/v) that encapsulates CuNPs (100 μg g^{-1}, 80 nm in size) and VC (10%). (b) The time course of the release of VC from an F-127 hydrogel. (c) The cytotoxicity of the F-127/CuNPs/VC hydrogel against HDFs by using the medium extraction method.

control hydrogel did not exhibit any discernable antibacterial effects for both *S. aureus* and *P. aeruginosa*. The F-127/CuNP/VC hydrogel resulted in significantly increased zone inhibition (15.31 ± 0.4 mm) in *S. aureus* compared to F-127/VC (7.07 ± 0.16 mm) or F-127/CuNPs gel (3.98 ± 0.1 mm) (Fig. 5a), suggesting a synergy between CuNPs and VC in conferring antibacterial effects. Similar responses were observed for *P. aeruginosa*, in which the zone inhibition for F-127/CuNP/VC hydrogel was measured to be 21.3 ± 0.58 mm, which was significantly higher than that of F-127/VC hydrogel (7.49 ± 0.63 mm) or F-127/CuNP hydrogel (4.19 ± 0.17 mm) (Fig. 5b). Interestingly, the antibacterial effect of F-127/VC hydrogel was greater than that of F-127/CuNP hydrogel, which appears to be a pro-oxidative property of VC at higher concentration. Taking together, our findings demonstrate the efficacy of the F-127/CuNPs/VC hydrogel in synergistically enhancing antibacterial effects against both Gram-positive and Gram-negative bacteria.

3.6. Antibiofilm efficacy of F-127/CuNPs/VC hydrogel

After observing the broad-spectrum antibacterial efficacy of F-127/CuNP/VC hydrogel and given the critical role of biofilm infection in the pathogenesis of wound chronicity,[4–6] we next assessed the efficacy of the F-127/CuNPs/VC hydrogel against bacterial biofilm using a colony biofilm model.[27] For this, colony biofilms were established by inoculating either *S. aureus* or *P. aeruginosa* bacteria onto a semi-permeable membrane atop of an agar plate (Fig. S5). This facilitated biofilm growth and the formation of stratified structures larger than those observed in other biofilm models by ensuring a continuous supply of nutrients.[41] The antibiofilm effect of the F-127/CuNPs/VC hydrogel was quantified by CFU counting and the results were compared with a F-127 hydrogel with CuNPs, F-127 with VC, and F-127 with a broad-spectrum antibiotic, *i.e.*, 1% ciprofloxacin (CIP). The antibiofilm effect of F-127/CuNPs or the F-127/VC hydrogel was negligible. The treatment of 1% CIP resulted in an approximately 2.5 log reduction in *S. aureus* biofilm, however, the CIP-loaded hydrogel was not effective against *P. aeruginosa* biofilm. In contrast, the treatment of the F-127/CuNP/VC hydrogel resulted in an approximately 7.5-log reduction of bacterial CFUs in both *S. aureus* and *P. aeruginosa* biofilms tested (Fig. 5c and d). These results demonstrate the potency of the F-127/CuNP/VC hydrogel in eradicating biofilm bacteria.

3.7. *In vivo* validation of F-127/CuNPs/VC hydrogel in a mouse model of skin wound infection

Finally, by observing the antibacterial and antibiofilm effects of F-127/CuNP/VC hydrogel *in vitro*, we sought to validate the

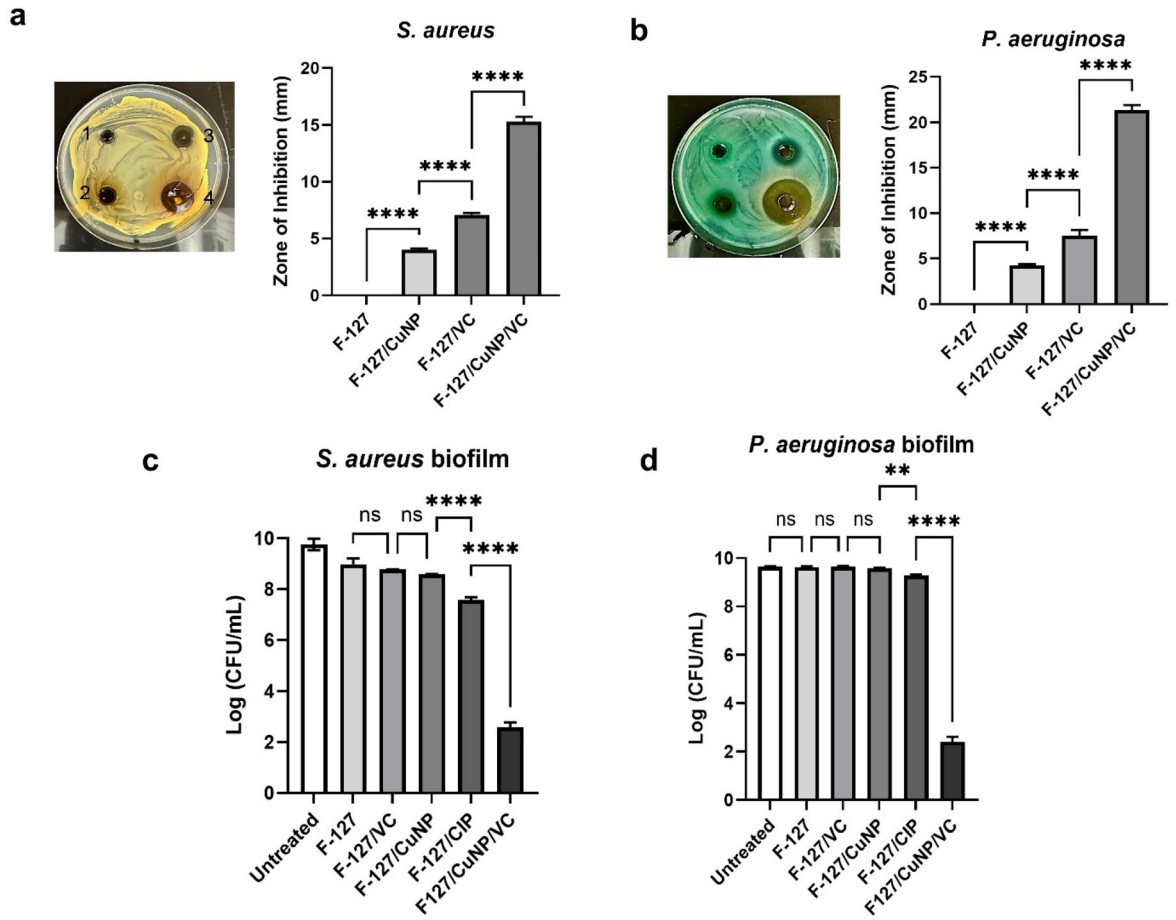

Fig. 5 Antibacterial and antibiofilm activities of the F-127/CuNPs/VC hydrogel against *S. aureus* and *P. aeruginosa*. (a and b) The antibacterial effect of the F-127/CuNPs/VC hydrogel against (a) *S. aureus* (ATCC 6538) and (b) *P. aeruginosa* (ATCC 15692) assessed by quantifying zone inhibition using a well diffusion assay. The results were compared with different F-127 hydrogel formulations including vehicle control (F-127 hydrogel), F-127 hydrogel with CuNPs only and F-127 hydrogel with VC only. (c and d) The effect of F-127/CuNP/VC hydrogel on the eradication of biofilm formed by (c) *S. aureus* (ATCC 6538) and (d) *P. aeruginosa* (ATCC 15692). The biofilm was formed by using a colony biofilm method and the extent of biofilm eradication was quantified by log colony forming units (log CFU). The results were compared with untreated control and different F-127 hydrogel formulations including vehicle control (F-127 hydrogel), F-127 hydrogel with CuNPs only, F-127 hydrogel with VC only, and F-127 hydrogel with 1% ciprofloxacin (CIP). $^{**}p < 0.01$, $^{****}p < 0.0001$. n.s: not significant.

anti-infective efficacy of the hydrogel *in vivo* using a murine model of skin wound infection colonized by either *S. aureus* or *P. aeruginosa*. For this, wild-type (Jax Swiss outbred) mice (male and female, 4–5 months old) were randomly assigned into four treatment groups ($n = 7$ per group): (1) *S. aureus* with F-127 vehicle control, (2) *S. aureus* with F-127/CuNPs/VC hydrogel, (3) *P. aeruginosa* with F-127 vehicle control, and (4) *P. aeruginosa* with F-127/CuNPs/VC hydrogel. Following a skin wounding procedure, mice were inoculated with 5×10^6 CFU mL^{-1} of bioluminescent *S. aureus* (Xen36, PerkinElmer) or *P. aeruginosa* (Xen41, PerkinElmer) in the skin wound site at day 0 (Fig. 6a). On day 1, either F-127/CuNPs/VC hydrogel or vehicle control (F-127 hydrogel only) was topically applied to the wound site of the treatment group. The hydrogels were topically applied once daily for 2 consecutive days. The changes in bacterial burden in the wound site were determined by measuring the bioluminescent signals of *S. aureus* and *P. aeruginosa* using an IVIS imaging system. The IVIS imaging continued through day 10 post-wounding and infection. The wound bacterial burden in mice treated with the control hydrogel remained high through day 3 for both *S. aureus* (Fig. 6b) and *P. aeruginosa* infections (Fig. 6c). In contrast, mice treated with F-127/CuNPs/VC hydrogel exhibited a marked and statistically significant reduction in bacterial burden as early as day 2, with sustained suppression of luminescence through day 10 for both *S. aureus* and *P. aeruginosa* infections.

Taken together, our findings support the feasibility of developing an F-127/CuNPs/VC hydrogel as an injectable wound dressing that can be topically applied for treating wound infections. The thermos-reversible property of F-127 gel made it facile for encapsulating a defined amount of CuNPs and VC into the gel, which is easily scalable for applying to larger wound areas.

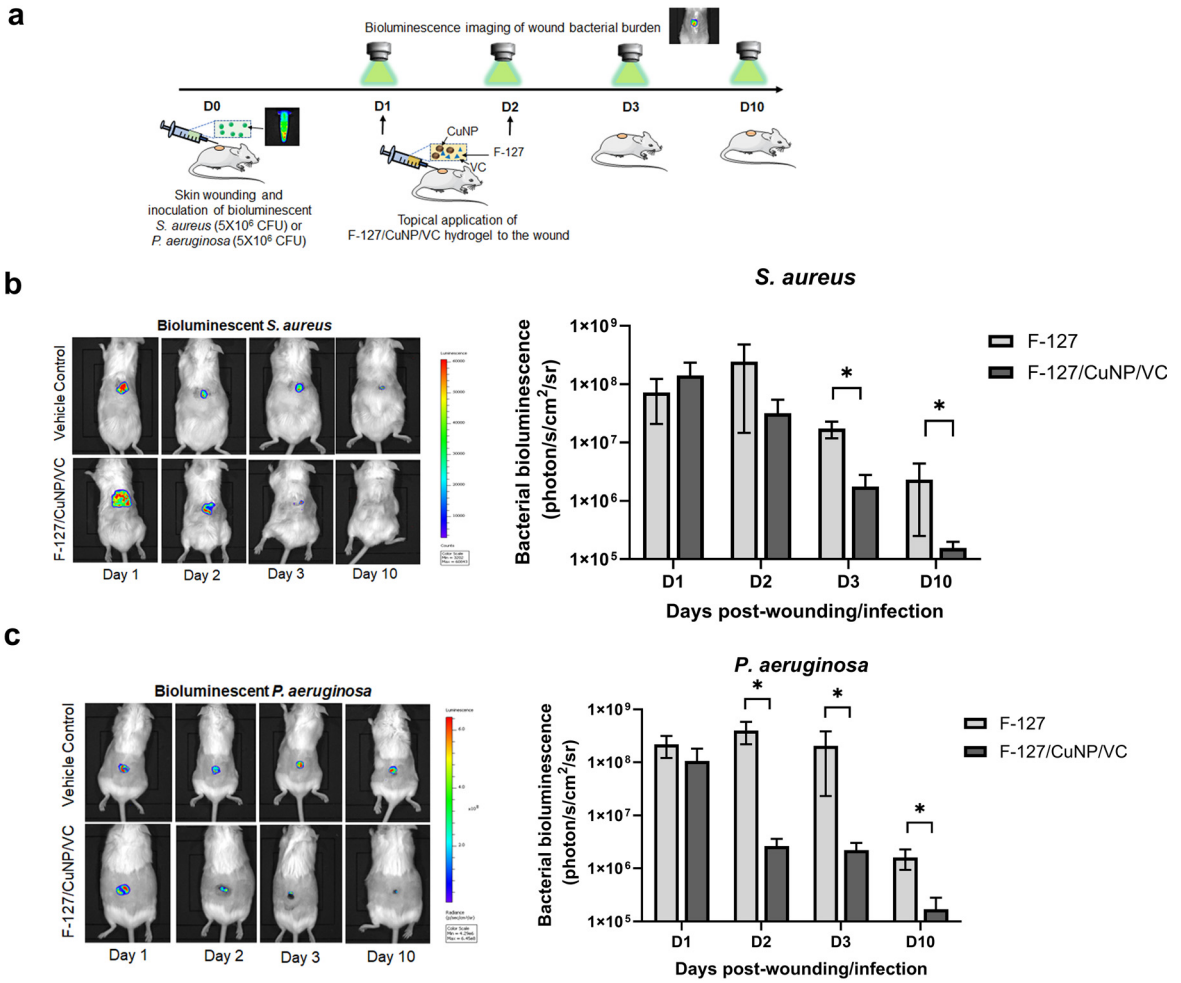

Fig. 6 Antibacterial activity of the F-127/CuNP/VC hydrogel against *S. aureus* and *P. aeruginosa* bacteria in a mouse model of skin infection. (a) Schematic representation of the experimental procedure for the treatment of F127/CuNPs/VC hydrogel to the wound of mice infected with *S. aureus* (ATCC 6538) or *P. aeruginosa* (ATCC 15692). (b and c) Representative images (left) and quantification (right) of (b) bioluminescent *S. aureus* and (c) bioluminescent *P. aeruginosa* in wounds of mice treated with either vehicle control (F-127 hydrogel) or F-127/CuNP/VC hydrogel. Number of mice: $N = 7$ for each group. Data are presented as the mean ± standard deviation (SD). Statistical analysis was performed using unpaired *t*-test. *: $p < 0.05$.

4. Conclusion

In summary, we demonstrated that harnessing the characteristic of CuNPs and VC to form a sustained catalytic cycle can provide a new strategy for treating skin bacterial infections. This study is based on the current understanding and scientific knowledge that (1) copper has great potential as an antimicrobial agent, while it is less harmful to the host cell because copper is an essential metal for life, and (2) VC can act as a co-drug (*i.e.*, a reducing agent) to form a sustaining Cu (0)/Cu(I)/Cu(II) redox cycle that boosts the production of cellular ROS. Our findings support that CuNPs, when properly combined with VC, can synergistically enhance antibacterial activity through the increased generation of intracellular ROS in bacterial cells. Additionally, our findings further support the feasibility of developing an F-127/CuNPs/VC hydrogel as a cost-effective and injectable scaffold for the management of wound infections.

However, it should be noted that our current F-127/CuNPs/VC hydrogel system needs to be further developed to be effective for wound healing applications. Firstly, the VC encapsulated in hydrogels can still be susceptible to rapid oxidation and degradation due to inherent instability of VC. The encapsulation of VC needs to be further optimized towards creating a more robust encapsulation system, minimizing degradation and enabling its controlled release. Secondly, while triggering the reaction between CuNPs and high dose of VC for ROS generation is beneficial for inflammatory phase of wound healing by facilitating the eradication of bacteria in the wound, this strategy is likely to interfere with smooth transitioning to the proliferative phase of wound healing since excessive ROS generation can be detrimental, leading to oxidative stress and delayed wound healing. It is necessary to further optimize the dosing of CuNPs and VC in the respective phase of wound healing towards exhibiting antibacterial activity as well as pro-angiogenic activity by means of, for instance, har-

nessing the dual functions of VC that displays either pro-oxidative or anti-oxidative response depending on its concentration.

Author contributions

Conceptualization, A. O., S. H., and M. K.; methodology, A. O., W. S., and M. K.; validation, A. O., and M. K.; formal analysis, A. O., and M. K.; investigation, A. O., T. H., and G. C.; resources, S. H., W. S., and M. K.; data curation, A. O., W. S., and M. K.; writing – original draft preparation, A. O., and M. K.; writing – review and editing, S. H., W. S., and M. K.; visualization, A. O., and M. K.; supervision, S. H., W. S., and M. K.; project administration, M. K.; funding acquisition, S. H., W. S., and M. K. All authors have read and agreed to the published version of the manuscript.

Conflicts of interest

The authors declare no competing financial interests.

Data availability

The data supporting this article have been included as part of the SI. Supplementary information is available. The content of supplementary information include supplementary table and figures. See DOI: **https://doi.org/10.1039/d5bm00933b**.

Any additional data requests should be made by contacting the corresponding author.

Acknowledgements

The TEM data reported in this work were obtained using the Cryo TEM Facility at the Advanced Materials and Liquid Crystal Institute, KSU. Patient clinical isolates of bacteria were kindly supplied by the VA Northeast Ohio Healthcare System.

References

1 O. A. Pena and P. Martin, *Nat. Rev. Mol. Cell Biol.*, 2024, **25**, 599–616.
2 G. C. Gurtner, S. Werner, Y. Barrandon and M. T. Longaker, *Nature*, 2008, **453**, 314–321.
3 M. Falcone, B. De Angelis, F. Pea, A. Scalise, S. Stefani, R. Tasinato, O. Zanetti and L. Dalla Paola, *J. Global Antimicrob. Resist.*, 2021, **26**, 140–147.
4 A. Omar, J. B. Wright, G. Schultz, R. Burrell and P. Nadworny, *Microorganisms*, 2017, **5**, 9.
5 M. Malone, T. Bjarnsholt, A. J. McBain, G. A. James, P. Stoodley, D. Leaper, M. Tachi, G. Schultz, T. Swanson and R. D. Wolcott, *J. Wound Care*, 2017, **26**, 20–25.
6 G. A. James, E. Swogger, R. Wolcott, E. Pulcini, P. Secor, J. Sestrich, J. W. Costerton and P. S. Stewart, *Wound Repair Regen.*, 2008, **16**, 37–44.
7 K. Gjodsbol, J. J. Christensen, T. Karlsmark, B. Jorgensen, B. M. Klein and K. A. Krogfelt, *Int. Wound J.*, 2006, **3**, 225–231.
8 V. Puca, R. Z. Marulli, R. Grande, I. Vitale, A. Niro, G. Molinaro, S. Prezioso, R. Muraro and P. Di Giovanni, *Antibiotics*, 2021, **10**, 1162.
9 S. L. Percival, C. Emanuel, K. F. Cutting and D. W. Williams, *Int. Wound J.*, 2012, **9**, 14–32.
10 E. Sanchez-Lopez, D. Gomes, G. Esteruelas, L. Bonilla, A. L. Lopez-Machado, R. Galindo, A. Cano, M. Espina, M. Ettcheto, A. Camins, A. M. Silva, A. Durazzo, A. Santini, M. L. Garcia and E. B. Souto, *Nanomaterials*, 2020, **10**, 292.
11 A. Girma, *Cell Surf.*, 2023, **10**, 100112.
12 K. Gold, B. Slay, M. Knackstedt and A. K. Gaharwar, *Adv. Ther.*, 2018, **1**, 1700033.
13 M. Vincent, R. E. Duval, P. Hartemann and M. Engels-Deutsch, *J. Appl. Microbiol.*, 2018, **124**, 1032–1046.
14 I. Salah, I. P. Parkin and E. Allan, *RSC Adv.*, 2021, **11**, 18179–18186.
15 S. R. Bharathi Devi, M. A. Dhivya and K. N. Sulochana, *J. Biosci.*, 2016, **41**, 487–496.
16 J. Barralet, U. Gbureck, P. Habibovic, E. Vorndran, C. Gerard and C. J. Doillon, *Tissue Eng., Part A*, 2009, **15**, 1601–1609.
17 A. N. Pham, G. W. Xing, C. J. Miller and T. D. Waite, *J. Catal.*, 2013, **301**, 54–64.
18 L. Chen, J. Min and F. Wang, *Signal Transduction Targeted Ther.*, 2022, **7**, 378.
19 S. Sathiyavimal, S. Vasantharaj, D. Bharathi, M. Saravanan, E. Manikandan, S. S. Kumar and A. Pugazhendhi, *J. Photochem. Photobiol., B*, 2018, **188**, 126–134.
20 M. E. Villanueva, A. M. Diez, J. A. Gonzalez, C. J. Perez, M. Orrego, L. Piehl, S. Teves and G. J. Copello, *ACS Appl. Mater. Interfaces*, 2016, **8**, 16280–16288.
21 T. Jayaramudu, K. Varaprasad, K. K. Reddy, R. D. Pyarasani, A. Akbari-Fakhrabadi and J. Amalraj, *Int. J. Biol. Macromol.*, 2020, **143**, 825–832.
22 J. Shen, P. T. Griffiths, S. J. Campbell, B. Utinger, M. Kalberer and S. E. Paulson, *Sci. Rep.*, 2021, **11**, 7417.
23 J. Kazmierczak-Baranska, K. Boguszewska, A. Adamus-Grabicka and B. T. Karwowski, *Nutrients*, 2020, **12**, 1501.
24 E. Gioffredi, M. Boffito, S. Calzone, S. M. Giannitelli, A. Rainer, M. Trombetta, P. Mozetic and V. Chiono, *Proc. CIRP*, 2016, **49**, 125–132.
25 J. Youn, J. H. Choi, S. Lee, S. W. Lee, B. K. Moon, J. E. Song and G. Khang, *Materials*, 2021, **14**, 1287.
26 H. Haidari, Z. Kopecki, R. Bright, A. J. Cowin, S. Garg, N. Goswami and K. Vasilev, *ACS Appl. Mater. Interfaces*, 2020, **12**, 41011–41025.
27 J. H. Merritt, D. E. Kadouri and G. A. O'Toole, in *Curr Protoc Microbiol*, 2005, chapter 1, unit 1B 1.
28 N. Abeydeera, B. M. Benin, K. Mudarmah, B. D. Pant, G. Chen, W. S. Shin, M. H. Kim and S. D. Huang, *Antibiotics*, 2023, **12**, 886.

29 A. Umer, S. Naveed, N. Ramzan, M. S. Rafique and M. Imran, *Materia*, 2014, **19**, 197–203.
30 Y. Li and M. A. Trush, *Carcinogenesis*, 1993, **14**, 1303–1311.
31 D. Meyerstein, *Nat. Rev. Chem.*, 2021, **5**, 595–597.
32 C. C. Winterbourn, *Nat. Chem. Biol.*, 2008, **4**, 278–286.
33 H. Kanafani and S. E. Martin, *J. Clin. Microbiol.*, 1985, **21**, 607–610.
34 W. S. da Cruz Nizer, V. Inkovskiy, Z. Versey, N. Strempel, E. Cassol and J. Overhage, *Pathogens*, 2021, **10**, 1187.
35 R. Dayer, B. B. Fischer, R. I. Eggen and S. D. Lemaire, *Genetics*, 2008, **179**, 41–57.
36 J. Fujii and Y. Ikeda, *Redox Rep.*, 2002, **7**, 123–130.
37 J. Fujii, T. Osaki and T. Bo, *Molecules*, 2022, **27**, 6187.
38 B. Shriky, A. Kelly, M. Isreb, M. Babenko, N. Mahmoudi, S. Rogers, O. Shebanova, T. Snow and T. Gough, *J. Colloid Interface Sci.*, 2020, **565**, 119–130.
39 S. Li, C. Yang, J. Li, C. Zhang, L. Zhu, Y. Song, Y. Guo, R. Wang, D. Gan, J. Shi, P. Ma, F. Gao and H. Su, *Int. J. Nanomed.*, 2023, **18**, 4485–4505.
40 F. Al-Niaimi and N. Y. Z. Chiang, *J. Clin. Aesthet. Dermatol.*, 2017, **10**, 14–17.
41 I. Guzman-Soto, C. McTiernan, M. Gonzalez-Gomez, A. Ross, K. Gupta, E. J. Suuronen, T. F. Mah, M. Griffith and E. I. Alarcon, *iScience*, 2021, **24**, 102443.